NANO LETTERS
Cite This: Nano Lett. XXXX, XXX, XXX−XXX
Letter
pubs.acs.org/NanoLett

Fully Quantized Electron Transfer Observed in a Single Redox Molecule at a Metal Interface

Antoine Roy-Gobeil,[†] Yoichi Miyahara,[*,†,¶] Kirk H. Bevan,[‡] and Peter Grutter[*,†]

[†]Department of Physics, McGill University, 3600 rue University, Montreal, Quebec H3A 2T8, Canada
[‡]Division of Materials Engineering, Faculty of Engineering, McGill University, Montreal, Quebec H3A 0C5, Canada

Supporting Information

ABSTRACT: Long-range electron transfer is a ubiquitous process that plays an important role in electrochemistry, biochemistry, organic electronics, and single molecule electronics. Fundamentally, quantum mechanical processes, at their core, manifest through both electron tunneling and the associated transition between quantized nuclear vibronic states (intramolecular vibrational relaxation) mediated by electron−nuclear coupling. Here, we report on measurements of long-range electron transfer at the interface between a single ferrocene molecule and a gold substrate separated by a hexadecanethiol quantum tunneling barrier. These redox measurements exhibit quantized nuclear transitions mediated by electron−nuclear coupling at 4.7 K in vacuum. By detecting the electric force associated with redox events by atomic force microscopy (AFM), with increasing AFM oscillation amplitude, the intensity of the observed cantilever resonance frequency shift peak increases and then exhibits a series of discrete steps that are indicative of quantized nuclear transitions. The observed peak shapes agree well with a single-electron tunneling model with quantized nuclear state transitions associated with the conversion of the molecule between oxidized and reduced electronic states. This technique opens the door to simultaneously investigating quantized electron and nuclear dynamics in a diverse range of systems.

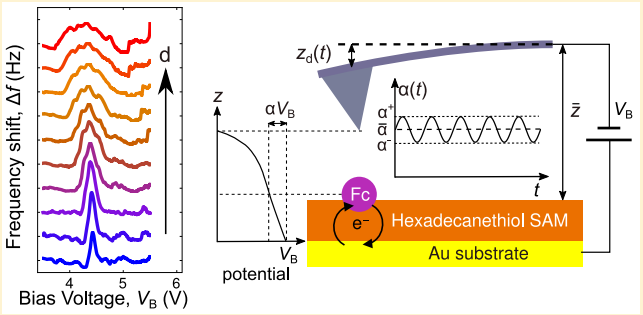

KEYWORDS: *electron transfer, Franck−Condon blockade, atomic force microscopy, single-electron tunneling, electron−vibron coupling, single-molecule electronics*

The quantum mechanical nature of electron tunneling in electron transfer processes has been extensively explored experimentally.[1] Though electron−nuclear coupling has been explored in state-of-the-art electron transport measurements[2−4] and a recent atomic force microscopy (AFM)-based measurement,[5] the quantum mechanical nature of nuclear vibronic state transition (nuclear quantization) driven by a change in the charge state has remained difficult to probe in electron transfer redox systems particularly at the single-molecule level.[6−12] Here we describe single-molecule low-temperature AFM measurements of nuclear quantization in heterogeneous electron transfer reactions between a ferrocene redox group and a gold electrode. Our measurements reveal quantized electron transfer energies corresponding to the eigenstates of a low lying vibronic mode, in excellent agreement with fully quantized (in terms of both electrons and nuclei) electron transfer theory.[13−15] This technique provides a new route toward exploring single-molecule electronic and nuclear quantization phenomena in electron transfer processes. In particular, we demonstrate experimentally and theoretically how AFM methods can be used to measure the molecule−metal electronic coupling strength, vibronic energies, and electron−nuclear coupling strengths that determine intramolecular reorganization energies.[13]

When expressing electron transfer (ET) quantum mechanically, one first invokes the Franck−Condon approximation, which enables one to separate the electronic coupling ($|M|^2$) and nuclear Franck−Condon factor in a transfer rate of the form

$$k_{mn} \approx \frac{2\pi}{\hbar} |M|^2 \, |\langle \chi_m | \chi_n \rangle|^2 \delta(E_m - E_n) \quad (1)$$

where χ_m and χ_n are the nuclear wave function components of the initial state and final state, respectively, belonging to vibronic states with energies E_m and E_n[6,7,14,16−19]—note, indices m and n indicate nuclear vibronic states and $\hbar$ is Planck's constant. Typically, the Franck−Condon factor $|\langle \chi_m | \chi_n \rangle|^2$ is thermally averaged at room temperature across many vibronic modes.[6,7,13] This allows the nuclear coordinates to be treated classically via Gerischer−Hopfield theory in terms of heterogeneous reactions at metal−molecule interfaces (or analogously in terms of Marcus−Hush theory in molecule−molecule reactions).[6,7,16,20−26] However, as we show here, at low temperatures (4.7 K) nuclear vibronic

Received: May 17, 2019
Revised: July 23, 2019
Published: August 20, 2019

DOI: 10.1021/acs.nanolett.9b02032
Nano Lett. XXXX, XXX, XXX−XXX

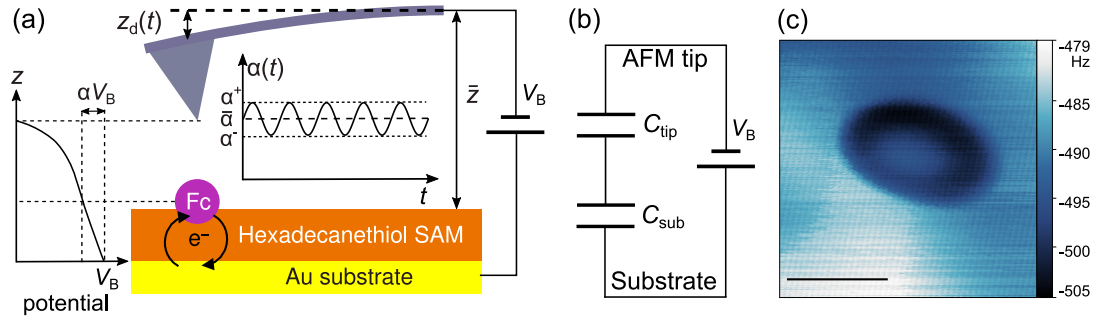

Figure 1. Electron transfer measured by electric force detection by AFM. (a) Schematic of the AFM experimental setup, x and y coordinates lie in the plane of the substrate, the voltage drop across the tunneling barrier (SAM layer) ($\alpha(x, y, z(t))V_B$) oscillates with the oscillating AFM tip position, $z(t) = \bar{z} + z_d(t) = \bar{z} + d\cos(2\pi f_0 t)$. α^+ and α^- indicate the maximum and minimum values of $\alpha(x, y, z(t))$. The electron transfer system probed consists of ferrocene-terminated alkanethiol molecules attached to a template-stripped gold surface. (b) Equivalent circuit diagram. (c) Frequency shift Δf measurement of a charging ring corresponding to a molecular level accessed at a fixed tip bias (V_B = 5.0 V). See body text for more detail about the formation of the ring. Scale bar is 30 nm.

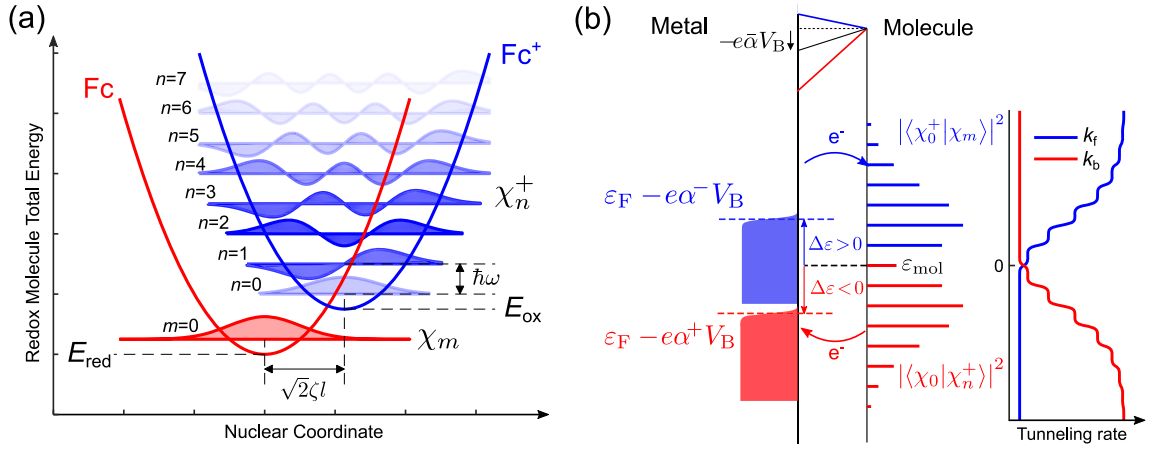

Figure 2. Theoretical model of electron transfer. (a) Total energy nuclear potentials of the Fc (red) and Fc^+ (blue) redox states with minima at E_{red} and E_{ox} (initially in the Fc configuration). The reduced (red) and oxidized (blue) states are shifted $\sqrt{2}\zeta$ in nuclear coordinates by the electron–phonon coupling parameter ζ. Transitions between reduced (χ_m) and oxidized (χ_n^+) nuclear states are determined by their coupling $\chi_m|\chi_n^+$. (b) (Left) Single-particle energy picture showing electrons in the metal distributed according to the Fermi–Dirac statistics, and the Franck–Condon factor weighted transition energies for oxidized (blue) and reduced (red) configurations of the molecule. Nuclear transitions are separated by discrete vibronic transitions in steps of $\hbar\omega$ about the molecular single-particle energy $\varepsilon_{mol} = E_{red} - E_{ox}$. Assuming full thermal relaxation, at 4.7 K electron transfer from and to the molecule occurs via the reduced and oxidized ground state nuclear wave functions ($n = 0$ and $m = 0$, respectively). (b) (Right) Associated forward (k_f) and backward (k_b) electron transfer rates as a function of the energy detuning, $\Delta\varepsilon$.

transitions are largely constrained to a single vibronic mode such that nuclear quantization becomes manifest in the allowable transition selection of $E_m = E_n$ in eq 1. This enables the experimental resolution of fully quantized single-molecule ET events at a metal–molecule interface in which quantized nuclear transitions enforce quantized ET energies as summarized by eq 1 (rather than a classical continuum of energies[6,16]).

Low temperatures present a considerable experimental obstacle when observing heterogeneous ET reactions, due to the consequential immobility of supporting electrolyte ions that typically accompany such reactions.[6] At room temperature, supporting electrolyte ions gate the single-particle eigenstates of a reactant enabling one to observe outer-sphere tunneling processes such as Coulomb blockade and rate saturation in heterogeneous ET experiments.[8−10,27,28] To overcome this difficulty, we have chosen to gate redox molecules in vacuum with a DC-biased AFM tip (see Figure 1a).[29−34] An AFM-based measurement enables one to measure ET for a single molecule in the absence of a solvent. A large contribution from the solvent to the total relaxation would make it difficult to observe relatively smaller intramolecular vibrational relaxation. Our redox system consists of ferrocene (Fc) tethered to a hexadecanethiol (16-ferrocenylhexadecanethiol, $Fc(CH_2)_{16}S$) self-assembled monolayer (SAM) on a template-stripped gold (see Methods for details regarding sample preparation).[8] Electron transfer between the substrate and the molecule is detected by mechanical charge sensing in vacuum using an oscillating AFM cantilever that is only capacitively coupled to the molecule.[29] The distance between the AFM tip and molecule is chosen to be approximately 10 nm such that no electron tunneling occurs between the tip and molecule, making this technique much less sensitive to the detail of the tip structure in contrast to scanning tunneling spectroscopy, which requires electron tunneling across two tunneling barriers (tip–molecule and molecule–metal substrate).

Based on the widely accepted capacitance model (Figure 1b),[35,36] a DC bias voltage, V_B, is applied between the AFM tip and substrate such that the voltage is split into two regions, one between the tip and molecule and another between the molecule and metal substrate (see Figure 1a). This results in a

DOI: 10.1021/acs.nanolett.9b02032
Nano Lett. XXXX, XXX, XXX−XXX

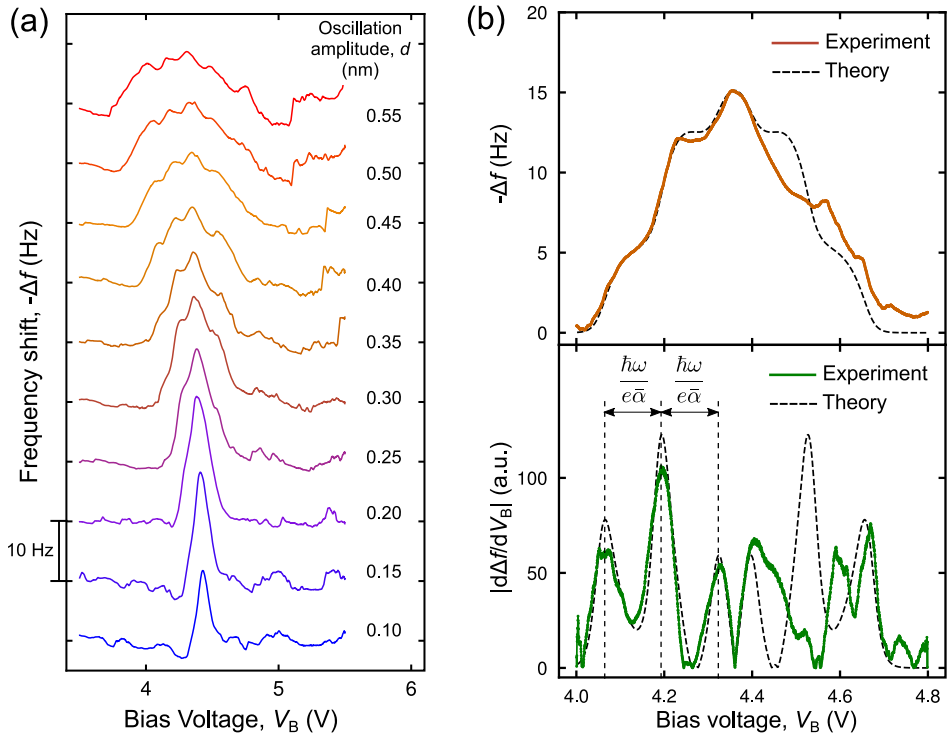

Figure 3. Frequency shift versus bias voltage spectroscopy. (a) Frequency shift (Δf) spectra, with increasing AFM oscillation amplitude, taken above a Fc group. The energy detuning, $\Delta\varepsilon$, becomes zero at $V_B \approx 4.4$ V around which a charging peak develops under small AFM tip oscillations. With increasing oscillation amplitude, the signal increases, indicating electron−vibron coupling. At high oscillation amplitudes, a larger tunneling energy window allows additional nuclear transitions, and discrete steps are observed. For data acquisition, the AFM tip was positioned at the center of the charging ring shown in Figure 1c with the tip−sample distance, $\bar{z} = 10$ nm. (b) AFM frequency shift response (top) and its derivative with respect to the bias voltage V_B (bottom) acquired at oscillation amplitude of $d = 0.35$ nm (solid line) compared with theory (dashed line) using the model parameters $\zeta = 1.6$ and $\hbar\omega = 11.6\ k_BT = 4.6$ meV. The lever-arm and its first derivative were calibrated to be $\alpha = 0.035$ and $A = -eV_B d\alpha/dz = 30.5$ meV/nm at $V_B = 4.4$ V, and the tunneling rate was measured to be 109.5 kHz.

voltage drop (overvoltage) of αV_B across the tunnel barrier between the metal substrate and the Fc terminated molecule of interest where α is the voltage splitting ratio (lever-arm). In this way, we control the energy difference (detuning) between the substrate Fermi energy, ε_F, and the single-particle level of the molecule, ε_{mol}, such as $\Delta\varepsilon = \varepsilon_F - e\alpha V_B - \varepsilon_{mol} = \Delta\varepsilon_0 - e\alpha V_B$ where $\Delta\varepsilon_0 \equiv \varepsilon_F - \varepsilon_{mol}$ is the energy level offset with $V_B = 0$ (Figure 2b).[27] When an appropriate bias voltage, $V_B^0 = \Delta\varepsilon_0/(e\alpha)$ is applied, the substrate Fermi energy is brought into resonance with a molecular single-particle eigenstate such that $\Delta\varepsilon = 0$.[24,27,28,32] The lever-arm, α, can be modeled by two capacitors connected in series (Figure 1b), one between the molecule and tip ($C_{tip}(x, y, z)$) and a second between the molecule and substrate (C_{sub}) as $\alpha(x, y, z) = C_{tip}(x, y, z)/[C_{tip}(x, y, z) + C_{sub}]$ where (x, y) and z indicate the lateral and vertical positions of the AFM tip with respect to the molecule, respectively. The capacitance model describes the energy detuning, which includes the voltage drop at the molecule in terms of α. We assume that the small changes in the potential drop inside the Fc part of the molecule do not alter its electronic structure and that the Fc molecular levels are lifted by αV_B with respect to the substrate (Figure 1a). As the lever-arm α can be experimentally determined in this AFM-based technique[30] (Supporting Information S3 for details), any particular capacitance model (e.g., planar) is not required for C_{tip} and C_{sub}.

When the tip is oscillated vertically at a certain position (x, y, z) near the molecule at a frequency of f_0 with an amplitude of d about a mean tip−molecule distance, $\bar{z}$, such as $z(t) = \bar{z} + d\cos(2\pi f_0 t)$, the energy detuning, $\Delta\varepsilon(x, y, z(t))$, likewise oscillates around its mean value, $\overline{\Delta\varepsilon}(x, y, \bar{z})$, through the oscillating $\alpha(x, y, z(t))$ as depicted in Figure 1a.[29,32] In this situation, the time-varying energy detuning, $\Delta\varepsilon(x, y, z(t))$, drives the alternating tunneling of an electron on (while $\Delta\varepsilon(x, y, z(t)) > 0$) and off (while $\Delta\varepsilon(x, y, z(t)) < 0$) the Fc group, causing the molecule to fluctuate between its oxidized (Fc^+) and reduced configuration (Fc) in response to the tip oscillation (Figure 2b and Supplementary Movie S1). Although the number of charges fluctuates due to the stochastic nature of tunneling, its average value follows the oscillating tip motion, subjecting the cantilever tip to an oscillating electrostatic force (Supplementary Movie S1).[34]

The average number of charges in the molecule is determined by the tunneling rates on and off through a rate equation[15,32] (see Supporting Information S1 for details). The in-phase component of the oscillating force with respect to the cantilever tip position leads to a detectable shift in the cantilever resonance frequency (Δf).[29,37,38] Scanning the tip over the sample at constant height (i.e., varying (x, y) with a fixed z) and with a fixed V_B produces rings of constant discharging/charging energy detuning ($\overline{\Delta\varepsilon}(x, y, \bar{z}) = \Delta\varepsilon_0 - e\alpha(x, y, \bar{z})V_B \approx 0$) in a Δf image (Figure 1c and Supplementary Figure S2) due to single-electron tunneling between a Fc group and gold surface through the SAM tunneling barrier. To explore fully quantized ET events, our AFM tip is placed at the center of the charging ring shown in Figure 1c with the average tip−sample separation of $\bar{z} = 10$ nm and Δf is recorded as a function of V_B. When the AFM tip oscillation amplitude is

DOI: 10.1021/acs.nanolett.9b02032
Nano Lett. XXXX, XXX, XXX−XXX

small (d = 0.1 nm), a sharp charging/discharging peak (Figure 3a) is observed in the Δf response at $V_B = V_B^0 \approx 4.4$ V, which is needed to situate the Fermi energy of the substrate at the resonance condition for the tip−sample distance chosen. This low oscillation amplitude corresponds to a very small amplitude of $\Delta\varepsilon(x, y, z(t))$ (~3 meV), whereby electrons are taken on/off the molecule directly at ε_{mol}. In this case, we can directly determine the electron tunneling rate through the SAM at the charging/discharging peak to be $0.752f_0$ = 109.5 kHz from the ratio of the measured in-phase response (Δf) to the quadrature cantilever response (often described as a dissipation signal in the AFM literature[29,32,38]—see Supporting Information S1.3 for more details). Upon increasing the AFM oscillation amplitude (d > 0.2 nm), which corresponds to increasing the amplitude of $\Delta\varepsilon(x, y, z(t))$, we observe marked discrete steps appearing in the Δf response as V_B are swept between 4 and 5 V (Figure 3a). These discrete steps in Δf, we argue, are a signature of ET quantized by the quantized nuclear degrees of freedom as expressed by eq 1.

To understand the origin of the discrete steps that appear as d (and thus the amplitude of $\Delta\varepsilon(x, y, z(t))$) is increased, we need to consider quantized nuclear vibronic transition. As shown in Figure 2a, at 4.7 K, the Fc group is initially in the nuclear ground state (χ_m with $m = 0$) in a nuclear potential represented by a parabola (red line in Figure 2a) with its energy, $E_{red} + \hbar\omega/2$ where ω is the vibronic frequency. After removing an electron to form Fc^+, the equilibrium nuclear coordinates shift by $\sqrt{2}\zeta$. Here we use a dimensionless representation in terms of the electron−nuclear coupling constant, ζ.[39] Within Gersicher−Hopfield theory, the heterogeneous reorganization energy, λ, of this mode can be expressed as $\lambda = \zeta^2\hbar\omega$.[21,24,25,39]

Removal of an electron to form Fc^+ requires a transition into one of the oxidized nuclear states χ_n^+ at $E_{ox} + \left(n + \frac{1}{2}\right)\hbar\omega$, the propensity of doing so is enforced by the Franck−Condon factor $|\langle\chi_m|\chi_n^+\rangle|^2$ as indicated by eq 1. A transition between the ground states (from m = 0 to n = 0) corresponds to the molecular single-particle energy, $\varepsilon_{mol} = E_{ox} - E_{red}$. Thus, a transition from m = 0 (in the reduced ground state) to n > 0 (in the oxidized state) corresponds to a single-particle energy of $\varepsilon_{mol} - n\hbar\omega$, with a weight of $|\langle\chi_0|\chi_n^+\rangle|^2$ as shown in red in Figure 2b. Similarly, allowed single-particle energies from the oxidized ground state n = 0 to reduced nuclear states at $m \geq 0$ are given by $\varepsilon_{mol} + m\hbar\omega$, with a propensity of $|\langle\chi_0^+|\chi_m\rangle|^2$ as shown in blue in Figure 2b. Given the measured tunneling rate of 109.5 kHz, we assume that a molecule fully relaxes thermally (at 4.7 K) before attempting a subsequent ET event.

As the amplitude of $\Delta\varepsilon(x, y, z(t))$ is increased, more single-particle transition states (at $\varepsilon_{mol} - n\hbar\omega$ and $\varepsilon_{mol} + m\hbar\omega$) appear within the tunneling energy window set by the maximum ($e\alpha^+V_B$) and minimum values ($e\alpha^-V_B$) of $e\alpha(x, y, z(t))V_B$ (left-hand side of Figure 2b). In the regime $\hbar\omega > k_BT$, this leads to an increased forward ET rate (k_f) in discrete steps of $\hbar\omega$ when $\Delta\varepsilon > 0$ and a similarly discretely increased backward ET rate (k_b) when $\Delta\varepsilon < 0$ as shown in Figure 2b and Supplementary Movie S2 (see Supplementary Equations S12 and S13 for detail)[16,24,39]—where k_BT is Boltzmann's constant multiplied by the system's temperature. Quantized changes in the ET rate at intervals of $\hbar\omega$ are manifest as changes in the Δf response of the oscillating AFM, resulting in the discrete steps observed in Figure 3a with increasing d (and correspondingly increasing $\Delta\varepsilon$ amplitude). Upon incorporating this quantized ET physics into our AFM model developed for quantum dot tunneling,[24,25,29−32,34,39] excellent theoretical agreement is obtained with the discrete steps observations (Figure 3b) (see Supporting Information S1 for details). Within our model, the voltage separation between the discrete steps in the Δf response can be quantitatively explained as arising due to quantized vibronic energies scaled by the mean value of α ($\equiv\bar{\alpha}$). By using the experimentally determined parameters of $\bar{\alpha}$ = 0.035 and $A = -eV_B d\alpha/dz$ = 30.5 meV/nm, we obtain an electron−nuclear coupling ζ = 1.6 and a vibronic energy $\hbar\omega = 11.6k_BT$ = 4.6 meV (see Supporting Information S3 for details). This vibronic energy agrees well with reported frequencies for the lowest-lying Fc vibrational mode, which fall around 4.0 ± 1.5 meV among inelastic neutron scattering, Raman, and infrared measurements.[40,41] Under the small perturbation applied by AFM gating, only the lowest-lying vibronic mode is excited. Accompanying transitions between higher vibronic modes are only between nuclear ground states under such small perturbations and therefore do not contribute to the spectra reported here.

These observations underscore that both nuclear and electron quantization are present in ET processes. At room temperature, ET nuclear transitions can be well approximated classically;[6,7,16,20−25] nevertheless, nuclear transitions remain fundamentally quantum mechanical (as illustrated by the low temperature measurements in this work). The single-molecule measurement of nuclear quantization via atomic force microscopy opens up the possibility of new fundamental nuclear dynamics insights into a wide range of ET problems across the fields of photochemistry, biochemistry, electrochemistry, and even electron transport. This includes exploring intriguing ET parallels to electron−nuclear coupled electron transport phenomena such as Franck−Condon blockade[2−4,39] and the charge transport in organic photovoltaic cells[42] and transistors.[43]

Methods. *Sample Preparation.* The sample was prepared by immersing a template-stripped gold substrate in a 1 mM solution of ferrocene tethered to hexadecanethiol (16-ferrocenylhexadecanethiol, $Fc(CH_2)_{16}S$) in ethanol for 48 h. After the incubation, the sample is rinsed with ethanol and blow-dried by nitrogen gas. See ref 32 for details on preparation of the template-stripped gold substrate and the self-assembled monolayer.

Detail of Low-Temperature Measurements. The measurements were performed with a home-built cryogenic AFM operated at 4.7 K.[44] A Pt-coated AFM cantilever (Nanosensors PPP-NCLR), with a spring constant of 20 N/m, was used. At 4.7 K, its quality factor was approximately 25 000 and its resonance frequency was f_0 = 146 kHz. During operation, the cantilever is oscillated at its resonance frequency, $z(t) = \bar{z} + d\cos(2\pi f_0 t)$ where $\bar{z}$ is the mean tip−sample distance, and the oscillation amplitude, d, is held constant by an automatic gain controller.[45] Cantilever deflection is detected by a fiber optic interferometer with a noise floor of 7 fm/$Hz^{1/2}$, operating with an RF-modulated 1550 nm wavelength laser diode.[46]

■ ASSOCIATED CONTENT

Supporting Information

The Supporting Information is available free of charge on the ACS Publications website at DOI: 10.1021/acs.nanolett.9b02032.

DOI: 10.1021/acs.nanolett.9b02032
Nano Lett. XXXX, XXX, XXX−XXX

Details of the theory; overview images of the sample; details of AFM energy calibration (PDF)

Movies of schematic representations of the electron transfer process for small (AVI) and large tip oscillation amplitude cases (AVI)

AUTHOR INFORMATION

Corresponding Authors

*E-mail: yoichi.miyahara@txstate.edu.

*E-mail: peter.grutter@mcgill.ca.

ORCID

Yoichi Miyahara: 0000-0002-9514-9603

Kirk H. Bevan: 0000-0001-9884-1403

Present Address

¶Department of Physics, Texas State University, San Marcos, Texas 78666, United States.

Author Contributions

Y.M. and P.G. conceived the experiment. A.R.-G. and Y.M. performed the measurements. A.R.-G., Y.M., and K.H.B. developed the theory. All authors discussed and wrote the manuscript.

Notes

The authors declare no competing financial interest.

ACKNOWLEDGMENTS

We thank A. A. Clerk for fruitful discussions. Funding for this research was provided by the Natural Sciences and Engineering Research Council of Canada and le Fonds Québécois de le Recherche sur la Nature et les Technologies.

REFERENCES

(1) Bixon, M.; Giese, B.; Wessely, S.; Langenbacher, T.; Michel-Beyerle, M. E.; Jortner, J. *Proc. Natl. Acad. Sci. U. S. A.* **1999**, *96*, 11713−11716.

(2) Qiu, X. H.; Nazin, G. V.; Ho, W. *Phys. Rev. Lett.* **2004**, *92*, 206102.

(3) Burzurí, E.; Yamamoto, Y.; Warnock, M.; Zhong, X.; Park, K.; Cornia, A.; van der Zant, H. S. J. *Nano Lett.* **2014**, *14*, 3191−3196.

(4) Lau, C. S.; Sadeghi, H.; Rogers, G.; Sangtarash, S.; Dallas, P.; Porfyrakis, K.; Warner, J.; Lambert, C. J.; Briggs, G. A. D.; Mol, J. A. *Nano Lett.* **2016**, *16*, 170−176.

(5) Fatayer, S.; Schuler, B.; Steurer, W.; Scivetti, I.; Repp, J.; Gross, L.; Persson, M.; Meyer, G. *Nat. Nanotechnol.* **2018**, *13*, 376−380.

(6) Schmickler, W. *Interfacial Electrochemistry*, 1st ed.; Oxford University Press, 1996.

(7) Balzani, V., Ed. *Electron Transfer in Chemistry*; Wiley-VCH Verlag GmbH, 2001.

(8) Chidsey, C. E. D. *Science* **1991**, *251*, 919−922.

(9) Fan, F.-R. F.; Bard, A. J. *Science* **1997**, *277*, 1791.

(10) Chen, S.; Ingram, R. S.; Hostetler, M. J.; Pietron, J. J.; Murray, R. W.; Schaaff, T. G.; Khoury, J. T.; Alvarez, M. M.; Whetten, R. L. *Science* **1998**, *280*, 2098−2101.

(11) Leoni, T.; Guillermet, O.; Walch, H.; Langlais, V.; Scheuermann, A.; Bonvoisin, J.; Gauthier, S. *Phys. Rev. Lett.* **2011**, *106*, 216103.

(12) Steurer, W.; Fatayer, S.; Gross, L.; Meyer, G. *Nat. Commun.* **2015**, *6*, 8353.

(13) Bixon, M.; Jortner, J. *Advances in Chemical Physics*; John Wiley & Sons, Inc., 1999; pp 35−202.

(14) Nitzan, A. *Chemical Dynamics in Condensed Phases: Relaxation, Transfer, and Reactions in Condensed Molecular Systems*; Oxford University Press, 2006.

(15) Koch, J.; von Oppen, F. *Phys. Rev. Lett.* **2005**, *94*, 206804.

(16) Ulstrup, J.; Jortner, J. *J. Chem. Phys.* **1975**, *63*, 4358−4368.

(17) Franck, J.; Dymond, E. G. *Trans. Faraday Soc.* **1926**, *21*, 536.

(18) Condon, E. *Phys. Rev.* **1926**, *28*, 1182−1201.

(19) Köuppel, H.; Domcke, W.; Cederbaum, L. S. *Advances in Chemical Physics*; John Wiley & Sons, Ltd, 2007; pp 59−246.

(20) Lax, M. *J. Chem. Phys.* **1952**, *20*, 1752−1760.

(21) Hopfield, J. J. *Proc. Natl. Acad. Sci. U. S. A.* **1974**, *71*, 3640.

(22) Marcus, R. A. *Rev. Mod. Phys.* **1993**, *65*, 599−610.

(23) Hush, N. S. *Trans. Faraday Soc.* **1961**, *57*, 557.

(24) Bevan, K. H.; Hossain, M. S.; Iqbal, A.; Wang, Z. *J. Phys. Chem. C* **2016**, *120*, 179.

(25) Bevan, K. H. *J. Chem. Phys.* **2017**, *146*, 134106.

(26) Bevan, K. H.; Roy-Gobeil, A.; Miyahara, Y.; Grutter, P. *J. Chem. Phys.* **2018**, *149*, 104109.

(27) Hossain, M. S.; Bevan, K. H. *J. Phys. Chem. C* **2016**, *120*, 188.

(28) Hossain, M. S.; Muralidharan, B.; Bevan, K. H. *J. Phys. Chem. C* **2017**, *121*, 18288.

(29) Miyahara, Y.; Roy-Gobeil, A.; Grutter, P. *Nanotechnology* **2017**, *28*, No. 064001.

(30) Cockins, L.; Miyahara, Y.; Bennett, S. D.; Clerk, A. A.; Studenikin, S.; Poole, P.; Sachrajda, A.; Grutter, P. *Proc. Natl. Acad. Sci. U. S. A.* **2010**, *107*, 9496−9501.

(31) Cockins, L.; Miyahara, Y.; Bennett, S. D.; Clerk, A. A.; Grutter, P. *Nano Lett.* **2012**, *12*, 709−713.

(32) Roy-Gobeil, A.; Miyahara, Y.; Grutter, P. *Nano Lett.* **2015**, *15*, 2324−2328.

(33) Stomp, R.; Miyahara, Y.; Schaer, S.; Sun, Q.; Guo, H.; Grutter, P.; Studenikin, S.; Poole, P.; Sachrajda, A. *Phys. Rev. Lett.* **2005**, *94*, No. 056802.

(34) Bennett, S. D.; Cockins, L.; Miyahara, Y.; Grütter, P.; Clerk, A. A. *Phys. Rev. Lett.* **2010**, *104*, No. 017203.

(35) Thijssen, J. M.; Van der Zant, H. S. J. *Phys. Status Solidi B* **2008**, *245*, 1455−1470.

(36) van der Wiel, W. G.; De Franceschi, S.; Elzerman, J. M.; Fujisawa, T.; Tarucha, S.; Kouwenhoven, L. P. *Rev. Mod. Phys.* **2002**, *75*, 1−22.

(37) Hölscher, H.; Gotsmann, B.; Allers, W.; Schwarz, U.; Fuchs, H.; Wiesendanger, R. *Phys. Rev. B: Condens. Matter Mater. Phys.* **2001**, *64*, No. 075402.

(38) Miyahara, Y.; Grutter, P. In *Kelvin Probe Force Microscopy: From Single Charge Detection to Device Characterization*; Sadewasser, S., Glatzel, T., Eds.; Springer International Publishing AG, 2018; Chapter 2.

(39) Koch, J.; von Oppen, F.; Andreev, A. V. *Phys. Rev. B: Condens. Matter Mater. Phys.* **2006**, *74*, 205438.

(40) Kemner, E.; de Schepper, I. M.; Kearley, G. J.; Jayasooriya, U. A. *J. Chem. Phys.* **2000**, *112*, 10926.

(41) Our system consists of ferrocene covalently tethered to hexadecanethiol; hence, agreement with isolated ferrocene vibrational measurements should not be exact.

(42) Song, P.; Li, Y.; Ma, F.; Pullerits, T.; Sun, M. *Chem. Rec.* **2016**, *16*, 734−753.

(43) Brédas, J.-L.; Beljonne, D.; Coropceanu, V.; Cornil, J. *Chem. Rev.* **2004**, *104*, 4971−5004.

(44) Roseman, M.; Grütter, P. *Rev. Sci. Instrum.* **2000**, *71*, 3782.

(45) Albrecht, T. R.; Grütter, P.; Horne, D.; Rugar, D. *J. Appl. Phys.* **1991**, *69*, 668−673.

(46) Rugar, D.; Mamin, H. J.; Guethner, P. *Appl. Phys. Lett.* **1989**, *55*, 2588−2590.

DOI: 10.1021/acs.nanolett.9b02032
Nano Lett. XXXX, XXX, XXX−XXX